Multimodal Approach to Detect Osseous Involvement in Meningioma: Additional Value of ^{18}F-Fluoride PET/CT for Conventional Imaging[1]

Ukihide Tateishi, MD
Kensuke Tateishi, MD
Ayako Hino-Shishikura, MD
Ikuo Torii, MD
Tomio Inoue, MD
Nobutaka Kawahara, MD

Purpose: To compare the diagnostic performance of fluorine 18 (^{18}F) fluoride positron emission tomography (PET)/computed tomography (CT) with that of conventional imaging (CT and magnetic resonance [MR] imaging) in evaluating the osseous involvement in meningioma.

Materials and Methods: The study was approved by the ethics committee and institutional review board and was conducted according to the Declarations of Helsinki and Tokyo. Written informed consent was obtained from all patients. A retrospective comparative study between ^{18}F-fluoride PET/CT and conventional imaging was conducted to detect osseous involvement in patients with a verified diagnosis of meningioma. Osseous involvement was verified by using definitive surgery (including drilling or careful sampling of the skull in all patients). The diagnostic performance, determined by calculating the sensitivity, specificity, positive predictive value (PPV), negative predictive value (NPV), and accuracy, was assessed.

Results: Data sets from a total of 78 patients with proven meningioma were compared. Osseous involvement was histopathologically confirmed in 25 patients (32%). The sensitivity, specificity, PPV, NPV, and accuracy were 92.0%, 86.8%, 76.7%, 95.8%, and 88.5% for ^{18}F-fluoride PET/CT and 64.0%, 83.0%, 64.0%, 83.0%, and 76.9% for conventional imaging, respectively. The receiver operating characteristic (ROC) analysis revealed that the area under the ROC curve (A_z) value of ^{18}F-fluoride PET/CT was significantly greater than that of conventional imaging (0.965 ± 0.02 [standard error] vs 0.703 ± 0.066 [standard error], $P < .0001$).

Conclusion: An approach using ^{18}F-fluoride PET/CT improves preoperative detection of osseous involvement. In those without abnormal ^{18}F-fluoride uptake within the skull, the patient may proceed directly to conventional surgery. However, a positive finding of osseous involvement at ^{18}F-fluoride PET/CT should prompt confirmation by drilling or sampling of bone.

[1]From the Departments of Radiology (U.T., A.H., I.T., T.I.) and Neurosurgery (K.T., N.K.), Yokohama City University Graduate School of Medicine, 3-9 Fukuura, Kanazawa-ku, Yokohama, Kanagawa 236-0004, Japan. Received September 18, 2013; revision requested November 11; final revision received February 3, 2014; accepted February 12; final version accepted May 20. Supported in part by the National Cancer Center Research and Development Fund (grant 23-A-25). **Address correspondence to** U.T. (e-mail: *utateish@yokohama-cu.ac.jp*).

Detection of osseous involvement in the care of patients with meningioma is necessary for proper surgical resection. In patients with operable tumors, the most substantial deciding factor for recurrence is the presence of osseous involvement, as resection of primary tumors and hyperostotic bone is needed for complete resection. Although hyperostosis can be detected by using conventional imaging (computed tomography [CT] and magnetic resonance [MR] imaging), conventional imaging often is a mediocre tool in differentiating between the presence and absence of osseous involvement, even if slight hyperostosis is identified (1–4).

Recently, positron emission tomography (PET) with the radiolabeled fluoride analog fluorine 18 (^{18}F) fluoride has been used in the assessment of osseous involvement in patients with meningioma (5). The results of our prior study suggest that increased ^{18}F-fluoride uptake in the skull adjacent to the primary tumor is associated with hyperostosis and osseous involvement. Therefore, ^{18}F-fluoride PET/CT is a promising noninvasive technique with particularly high sensitivity for detection of hyperostosis and osseous involvement in patients with meningioma. However, the diagnostic performance of ^{18}F-fluoride PET/CT has not been compared with that of the conventional imaging alone in evaluating osseous involvement in meningioma, and the role of ^{18}F-fluoride PET/CT in the detection of osseous involvement in patients with meningioma should be clarified.

The aim of the current study was to compare the diagnostic performance of ^{18}F-fluoride PET/CT with that of conventional imaging in evaluating the osseous involvement in meningioma.

Advances in Knowledge

- ^{18}F-fluoride PET/CT improves preoperative detection of osseous involvement in patients with meningioma, with sensitivity of 92.0%, specificity of 86.8%, and accuracy of 88.5%.
- A positive finding at ^{18}F-fluoride PET/CT should prompt confirmation of osseous involvement by drilling or sampling of bone.

Materials and Methods

Patients

A total of 78 patients between 11 and 83 years of age with histopathologically proven meningioma were retrospectively assessed from December 2011 to December 2013. Of these, 67 patients (86%) had primary meningiomas and 11 patients (14%) had recurrent tumors. The initial assessment in all patients was based on medical history, physical examinations, and conventional imaging studies that included CT and MR imaging. The criterion for eligibility for this study was World Health Organization performance status 0 or 1. Patients with uncontrolled diabetes (n = 1), pregnancy (n = 1), apparent infection (n = 1), other serious medical disorders (n = 2), or concomitant malignancy (n = 5) were excluded. The study was approved by the Ethics Committee and Institutional Review Board of Yokohama City University Hospital, Yokohama, Japan (No. B1001111026), and was conducted according to the Declarations of Helsinki and Tokyo. Written informed consent was obtained from all patients.

Conventional Imaging

Conventional imaging consisted of CT and MR studies. CT studies were performed within 5 days before ^{18}F-fluoride PET/CT and 10 days before surgery. CT was performed by using a 64–detector row multisection system (Aquilion 64; Toshiba Medical Systems, Ohtawara, Tochigi, Japan), with the following parameters: 120 kVp, 350 mA, 1-mm section thickness with 64 detector rows, nonhelical scan, reconstruction thickness of 4 mm, and function code 64 (FC64; Toshiba Medical Systems). Contrast material–enhanced CT was performed after administration of contrast medium (Iopamiron; Bayer, Berlin, Germany), 300 mg iodine, at a rate of 1.0 mL/sec with an automatic injector (Dual Shot; Nemoto-Kyorindo, Tokyo, Japan) with a scan delay of 90 seconds. MR studies were performed within a week before ^{18}F-fluoride PET/CT and 11 days before surgery. MR imaging was performed by using a 1.5-T system (Magnetom Symphony, Siemens, Erlangen, Germany; or Gyroscan Intera Master, Philips Medical Systems, Best, the Netherlands). Pulse sequences, including T1-weighted spin-echo imaging, T2-weighted fast spin-echo imaging, diffusion-weighted spin-echo imaging, as well as contrast-enhanced T1-weighted spin-echo imaging with fat suppression, were used as previously described (5).

Implication for Patient Care

- ^{18}F-fluoride PET/CT should be performed in all patients with meningioma who are being considered for surgery.

PET/CT Studies

^{18}F-fluoride was produced by irradiating oxygen 18 water with protons in a metal target and was trapped by passing the target water through an anion exchange resin, which was the same method we described previously (5). A phantom PET/CT study was performed to clarify the necessary and sufficient conditions for data acquisition and to ensure quality control before the clinical study (6).

Published online before print
10.1148/radiol.14132118 **Content codes:** NM NR CT MR

Radiology 2014; 273:521–528

Abbreviations:
A_z = area under the ROC curve
BMP-4 = morphogenetic protein 4
MTV = metabolic tumor volume
NPV = negative predictive value
PPV = positive predictive value
ROC = receiver operating characteristic
SUV = standardized uptake value
TBM = total bone metabolism

Author contributions:
Guarantors of integrity of entire study, U.T., A.H.; study concepts/study design or data acquisition or data analysis/interpretation, all authors; manuscript drafting or manuscript revision for important intellectual content, all authors; approval of final version of submitted manuscript, all authors; literature research, U.T., K.T., A.H., N.K.; clinical studies, all authors; experimental studies, K.T., A.H.; statistical analysis, U.T., A.H., N.K.; and manuscript editing, U.T., K.T., A.H., N.K.

Conflicts of interest are listed at the end of this article.

Studies were performed by using a whole-body PET/CT scanner (Aquiduo PCA-7000B; Toshiba Medical Systems) equipped with a CT component having 16 detector rows. We used a BT phantom for cross calibration. All patients received an intravenous injection of 3.7 MBq/kg of ^{18}F-fluoride after fasting at least 6 hours and resting for 1 hour. The mean uptake time was 50 minutes ± 6 (standard deviation). Scanning parameters for PET/CT were as follows: data acquisition, 120 seconds per bed; field of view, 500 mm; iterations, four; subsets, 14; matrix size, 128 × 128; filter, Gaussian 8 mm in full width at half maximum; and reconstruction, attenuation-weighted ordered-subsets expectation maximization. For the CT portion of the examination, low-dose CT data were acquired at 120 kVp using an automatic exposure control system, a beam pitch of 0.875 or 1, and a 16–detector row mode with 1.5- or 2-mm section thickness.

Image Interpretation

Conventional images were evaluated by two board-certified radiologists (I.T., with 9 years of experience, and A.H., with 10 years of experience) separately with clinical information. Within-group interpreter agreement was assessed by using the Cohen κ and the McNemar test. CT and MR findings of the skull adjacent to the primary tumor were assessed by using a workstation (Synapse; Fujifilm Medical, Tokyo, Japan). A representative case for image interpretation is presented in Figure 1. When a mass or a masslike lesion of the skull adjacent to the primary tumor was identified at CT or MR imaging, osseous involvement was considered to be positive. On a CT scan, the presence or absence of sclerotic or lytic changes was counted. The patterns of signal intensity of osseous involvement on T1-weighted, T2-weighted, diffusion-weighted, and contrast-enhanced T1-weighted images were collected for evaluation of MR images.

PET/CT images were assessed by two board-certified nuclear medicine specialists (U.T., with 19 years of experience, and T.I., with 37 years of experience) separately, with clinical information. Within-group interpreter agreement was also evaluated by using the Cohen κ and the McNemar test. The PET and CT images were reviewed on a workstation (PETSTAT, Adin Research, Tokyo, Japan) in all standard planes. When increased uptake greater than that in the normal skull is identified in the skull adjacent to the primary tumor, osseous involvement was considered to be positive (Fig 1). A volume of interest was outlined within areas of increased uptake and was measured on each section. When the lesion was extensively heterogeneous, the volume of interest was set to cover all of the components of the lesion. When the tumor was located in the center of the skull, we referred to the frontal bone. The standardized uptake value (SUV) was calculated according to the following equation: $SUV = [(C_{max} \cdot F_{cal})/A_{inj}]/BW$, where C_{max} is maximum count, F_{cal} is calibration factor in kilobecquerels per milliliter, A_{inj} is injected activity in megabecquerels, and BW is body weight in kilograms. Maximum values were used to minimize the partial volume effects and to increase the reproducibility of the measurements. Metabolic tumor volume (MTV) was calculated on the basis of the gross tumor volume on the PET scan. Total bone metabolism (TBM) was calculated as the product of MTV and average SUV.

Histopathologic Evaluation

Samples from the tumor and the skull were obtained at the time of definitive surgery (drilling or careful sampling of the skull). Merged PET/CT images were exported to a neuronavigation system (StealthStation; Medtronic Sofamor Danek, Memphis, Tenn) for precise tissue sampling. When an osseous lesion was considered to be difficult to remove at surgery, drilling or careful sampling of the lesion from the center and periphery of the bone flap representing strong accumulation of ^{18}F-fluoride was performed. Histologic sections 4 μm in thickness were cut, stained with hematoxylin-eosin, and examined with light microscopy. Tumor specimens were immunostained with the Ki-67 antibody (clone MIB-1; Dako Cytomation, Glostrup, Denmark), diluted in a ratio of 1:100, and autoclaved, and the Ki-67 (MIB-1; Dako Cytomation) labeling index was similarly estimated with the methods we described previously (5). The mean interval between the PET/CT study and either surgical resection or biopsy was 12.5 days (range, 1–17 days). Follow-up MR imaging was performed at 6 and 12 months after surgery in all patients.

Statistical Analysis

The primary analysis was of the diagnostic performance of ^{18}F-fluoride PET/CT and that of conventional imaging to detect osseous involvement. The performance was assessed by calculating the sensitivity, specificity, positive predictive value (PPV), negative predictive value (NPV), and accuracy with corresponding 95% confidence intervals (exact method that was based on the binomial distribution). The sensitivity and specificity are defined as the number of true-positive decisions of osseous involvement divided by the number of actually positive cases with osseous involvement and the number of true-negative decisions of osseous involvement divided by the number of actually negative cases with osseous involvement, respectively. PPV is defined as the probability of osseous involvement among patients with a positive result at PET/CT or conventional imaging. NPV is defined as the probability of no osseous involvement among patients with a negative result at PET/CT or conventional imaging. The differences in sensitivity, specificity, PPV, NPV, and accuracy were compared between ^{18}F-fluoride PET/CT and conventional imaging by using the receiver operating characteristic (ROC) analysis. The area under the ROC curve (A_z) is defined as the average value of sensitivity for all possible values of specificity for osseous involvement by using PET/CT or conventional imaging. The ROC curve is obtained by plotting the sensitivity of a test on the y-axis against one minus specificity on the x-axis (7). We calculated the A_z value. In general, the closer the A_z value is to one, the better the overall diagnostic

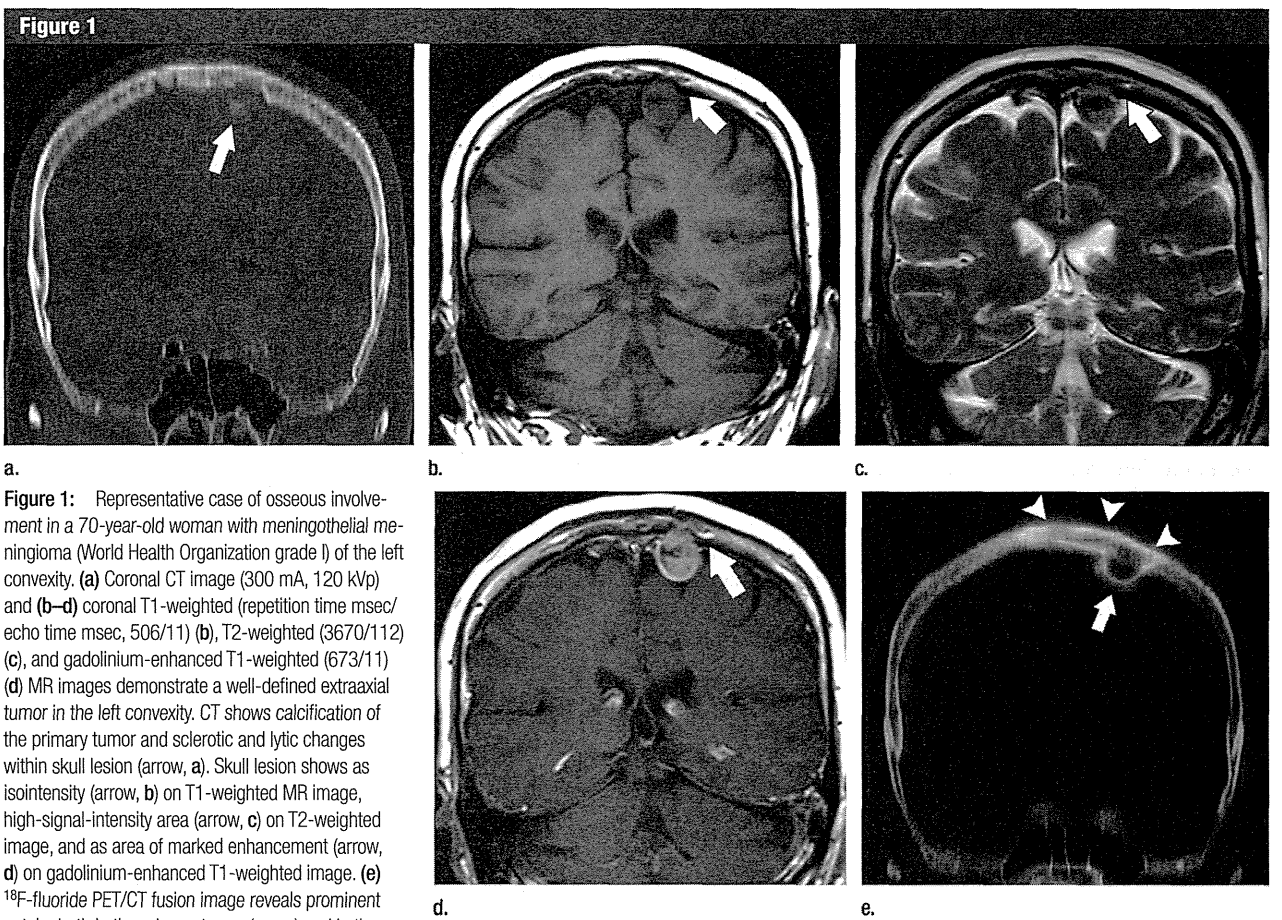

Figure 1: Representative case of osseous involvement in a 70-year-old woman with meningothelial meningioma (World Health Organization grade I) of the left convexity. **(a)** Coronal CT image (300 mA, 120 kVp) and **(b–d)** coronal T1-weighted (repetition time msec/echo time msec, 506/11) **(b)**, T2-weighted (3670/112) **(c)**, and gadolinium-enhanced T1-weighted (673/11) **(d)** MR images demonstrate a well-defined extraaxial tumor in the left convexity. CT shows calcification of the primary tumor and sclerotic and lytic changes within skull lesion (arrow, **a**). Skull lesion shows as isointensity (arrow, **b**) on T1-weighted MR image, high-signal-intensity area (arrow, **c**) on T2-weighted image, and as area of marked enhancement (arrow, **d**) on gadolinium-enhanced T1-weighted image. **(e)** ^{18}F-fluoride PET/CT fusion image reveals prominent uptake both in the primary tumor (arrow) and in the skull containing osseous involvement (arrowheads). Normal skull shows minimal uptake.

performance of the test. The difference of A_z value was compared with a χ^2 test by using the theory on generalized U statistics to generate an estimated covariance matrix (8). The variables were compared by using hypothesis testing for proportions in two independent groups, assuming normal distribution of the differences and without continuity correction. Clinical characteristics were compared with the use of an independent t test for continuous variables and a χ^2 test or Fisher exact test for mutually exclusive categorical variables. Comparison of the PET/CT measurements between patients with or without osseous involvement was performed by using the Student t test. Within-group interpreter agreement was measured by using the Cohen κ and the McNemar test. The κ values were interpreted thus: less than 0.20, poor agreement; 0.21–0.40, fair agreement; 0.41–0.60, moderate agreement; 0.61–0.80, good agreement; and 0.81–1.00, excellent agreement. All reported P values were two sided, and a significance level of .05 was applied. For the statistical tests, we used a two-sided significance level of .05. Statistical analysis was performed with software (PASW Statistics 19, IBM, Tokyo, Japan; and SAS, version 9.2 for Windows, SAS Institute, Cary, NC).

Results

Demographics in patients are presented in Table 1. Osseous involvement was identified in 25 of 78 patients (32%). Eighty-six percent of patients had no initial symptoms. Meningothelial meningioma was the most frequently occurring histopathologic subtype, followed by transitional meningioma, fibrous meningioma, and atypical meningioma. The most frequent World Health Organization grade of the tumor was grade I. Locations of the tumor included the convexity, middle cranial fossa, parasagittal, cerebellar convexity, and tentorium cerebelli. Osseous involvement was stratified according to primary tumor size and calcification of the main tumor.

The Cohen κ values of CT, MR imaging, and ^{18}F-fluoride PET/CT were 0.74, 0.83, and 0.77, respectively. CT revealed that most lesions of osseous involvement showed sclerotic change (Table 2). Specific MR signal intensity patterns of lesions with osseous

Table 1

Demographics in 78 Patients

Characteristic	With Osseous Involvement	Without Osseous Involvement	*P* Value
All patients	25 (32)	53 (68)	
Male patients	13 (17)	21 (27)	.304
Female patients	12 (15)	32 (41)	
Age (y)*	61 ± 2	57 ± 2	.218
Size of primary tumor (mm) *	44 ± 4	31 ± 2	.001
Malignant tumor	3 (4)	2 (3)	.32
Recurrent tumor	3 (4)	8 (10)	>.99
Chief complaint			.259
Headache	4 (5)	4 (5)	
Vertigo	1 (1)	1 (1)	
Gait disturbance	1 (1)	0	
None	19 (24)	48 (62)	
Histopathologic subtype			.773
Meningothelial	13 (17)	34 (44)	
Transitional	6 (8)	10 (13)	
Fibrous	3 (4)	4 (5)	
Atypical	3 (4)	5 (6)	
Location			.067
Convexity	14 (18)	17 (22)	
Parasagittal	2 (3)	10 (13)	
Middle cranial fossa	5 (6)	10 (13)	
Cerebellar convexity	4 (5)	6 (8)	
Tentorium cerebelli	0	10 (13)	
Calcification of main tumor	10 (13)	4 (5)	.027

Note.— Except where otherwise indicated, data are numbers of patients, and numbers in parentheses are percentages. Percentages were rounded.

* Data are means ± standard deviations.

Table 2

Conventional Imaging Findings of Lesions with Osseous Involvement in 25 Patients

Findings	No. of Patients
CT pattern	
Sclerotic	9 (36)
Sclerotic and lytic	9 (36)
Normal	7 (28)
MR signal intensity pattern	
T1W image	
Hypointense	12 (48)
Isointense	13 (52)
Hyperintense	0
T2W image	
Hypointense	0
Isointense	13 (52)
Hyperintense	12 (48)
CE T1W image	
No enhancement	12 (48)
Abnormal enhancement	13 (52)
DW image	
Negative	21 (84)
Positive	4 (16)

Note.—CE = contrast-enhanced, DW = diffusion weighted, T1W = T1 weighted, T2W = T2 weighted. Numbers in parentheses are percentages. Percentages were rounded.

involvement were not identified. The contribution of diffusion-weighted imaging to detect osseous involvement was limited (Table 2).

All PET/CT measurements of the main tumor, including maximum SUV, MTV, and TBM, were similar for lesions with or without osseous involvement (Table 3). The mean ± standard deviation of maximum SUV, MTV, and TBM of the lesion with osseous involvement were 13.2 ± 1.1, 32.4 ± 10.4, and 358.8 ± 142.9, respectively. Significant differences between the main tumor and the lesion with osseous involvement were identified in maximum SUV ($P < .0001$) and MTV ($P = .013$), respectively. By contrast, the difference in TBM between lesions with and without osseous involvement was marginal.

Table 3

^{18}F-Fluoride PET/CT Measurements in Primary Tumor

Primary Tumor	With Osseous Involvement	Without Osseous Involvement	*P* Value
Maximum SUV (g/mL)	7.8 ± 3.9	7.2 ± 5.3	.602
MTV (mL)	14.8 ± 8.6	7.5 ± 11.7	.251
TBM (g)	115.7 ± 91.3	57.3 ± 17.8	.39

Note.—Data are means ± standard deviations, except where otherwise indicated.

At ^{18}F-fluoride PET/CT, histopathologic specimens obtained by drilling showed negative results in two patients (3%) regardless of osseous involvement. The mean size of these lesions was 7 mm in the largest diameter. False-positive findings were found in seven patients (9%) at ^{18}F-fluoride PET/CT, and histopathologic specimens revealed hyperostotic changes in all these lesions. The osseous involvement findings were false-positive in nine patients (12%) and false-negative in nine patients (12%) by using conventional imaging. The mean size of the false-negative lesions was 10 mm in the largest diameter. Histopathologic findings in patients with false-positive results were hyperostosis in seven patients (9%) and normal or heterogeneous bone marrow in two patients (3%).

The sensitivity, specificity, PPV, NPV, and accuracy of osseous involvement detection for ^{18}F-fluoride PET/CT

Table 4

Diagnostic Performance of ^{18}F-Fluoride PET/CT and Conventional Imaging for Detection of Osseous Involvement

Method	Sensitivity	Specificity	PPV	NPV	Accuracy
^{18}F-fluoride PET/CT	92.0 (74.0, 99.0)	86.8 (74.7, 94.5)	76.7 (57.7, 90.1)	95.8 (85.8, 99.5)	88.5 (79.2, 94.6)
Conventional imaging	64.0 (42.5, 82.0)	83.0 (70.2, 91.9)	64.0 (42.5, 82.0)	83.0 (70.2, 91.9)	76.9 (66.0, 85.7)

Note.—Data are percentages, and percentages were rounded. Numbers in parentheses are 95% confidence intervals.

and conventional imaging are presented in Table 4. Compared with the conventional imaging strategy, the ^{18}F-fluoride PET/CT strategy appears to have a slightly superior sensitivity, NPV, and accuracy of osseous involvement detection (Fig 2). The ROC analysis revealed that the mean A_z value of ^{18}F-fluoride PET/CT was significantly greater than that of conventional imaging (0.965 ± 0.02 [standard error], with 95% confidence interval: 0.930, 1.000, vs 0.703 ± 0.066 [standard error], with 95% confidence interval: 0.574, 0.832) with $P < .0001$ (Fig 3). The between-group difference in sensitivity, specificity, PPV, NPV, and accuracy was not significant if the data were stratified according to malignant tumor, recurrent tumor, histopathologic subtype, and location.

Discussion

Our study results demonstrate that the accuracy of osseous involvement detection by using ^{18}F-fluoride PET/CT appears to be superior to that by using conventional imaging. The addition of ^{18}F-fluoride PET/CT to the preoperative evaluation can reveal information about occult osseous involvement and aid selection of the surgical margin. These findings suggest that ^{18}F-fluoride PET/CT should be performed in all patients with meningioma who are being considered for surgery.

True mechanisms responsible for ^{18}F-fluoride uptake in meningioma are not fully established. ^{18}F-fluoride ions exchange with hydroxyl groups in the hydroxyapatite crystal bone to form ^{18}F-fluoroapatite within tumors. Our own previous study on meningioma has shown that uptake of ^{18}F-fluoride within tumor or adjacent bone may reflect regional blood flow, active bone formation, and osseous turnover (5). We previously assessed the capability of ^{18}F-fluoride PET/CT to help detect occult osseous involvement by determining whether differences in diagnostic performance between the ^{18}F-fluoride PET/CT group and the control patients (conventional imaging group) were explicable. One basic study (9) in which the researchers were investigating bone formation in meningiomas demonstrated that osteopontin, a 38-kDa phosphorylated glycoprotein secreted by macrophage, induced the development of psammoma bodies and was bound to calcium phosphate, which is associated with ^{18}F-fluoride uptake in meningioma. The investigators (9) also suggested that bone morphogenetic protein 4 (BMP-4), one of the growth factors regulating formation of bone from mesoderm, might play autocrine and paracrine roles in the growth and differentiation of meningioma. Another investigator (10) reported that the autocrine effect of BMP-4 could sustain tumor growth in meningioma and that the paracrine effect of BMP-4 contributed to hyperostosis and osseous involvement in the overlying skull. We hypothesize, but cannot prove, that osteopontin and BMP-4 may interact with ^{18}F-fluoride and affect its uptake in meningioma. Further studies of the correlation between ^{18}F-fluoride uptake and expression of osteopontin and BMP-4 are warranted to clarify the role of calcium metabolism in meningioma.

Notably, osseous involvement is frequently identified in meningioma (11–14). However, detection of osseous involvement might be difficult to achieve as a part of the daily clinical routine for screening because the results of the previous imaging studies demonstrated low sensitivity (1–4,15). The extent of proven osseous involvement appears as areas of abnormal accumulation at technetium 99m (^{99m}Tc) methylene diphosphonate scintigraphy (16–18). Although the mechanisms of ^{18}F-fluoride and ^{99m}Tc–methylene diphosphonate uptake in fluoroapatite of osseous lesions are similar, the findings of the previous studies in which the researchers evaluated the capability of individual imaging modalities or the differences between modalities, including single photon emission computed tomography (SPECT), SPECT/CT, and PET/CT, to aid detection of osseous involvement are limited. Further research is required to determine whether or not there is indeed an incremental diagnostic improvement with ^{18}F-fluoride PET/CT over other imaging methods, including ^{99m}Tc–methylene diphosphonate SPECT/CT.

Investigators in many studies demonstrate that tracer uptake is correlated with tumor grade and is linked to tumor grade or aggressiveness in meningioma (6,19–23). In our previous study, we similarly showed the association between continuous measurement of ^{18}F-fluoride or ^{18}F-fluorodeoxyglucose uptake and tumor grade in meningioma (5) and significantly greater differences in maximum SUV and MTV in lesions with osseous involvement than in lesions without osseous involvement at ^{18}F-fluoride PET/CT. These data suggest that continuous measurements of PET/CT may help identify osseous involvement in meningioma.

Potential limitations of the study include retrospective comparisons of limited cases with osseous involvement.

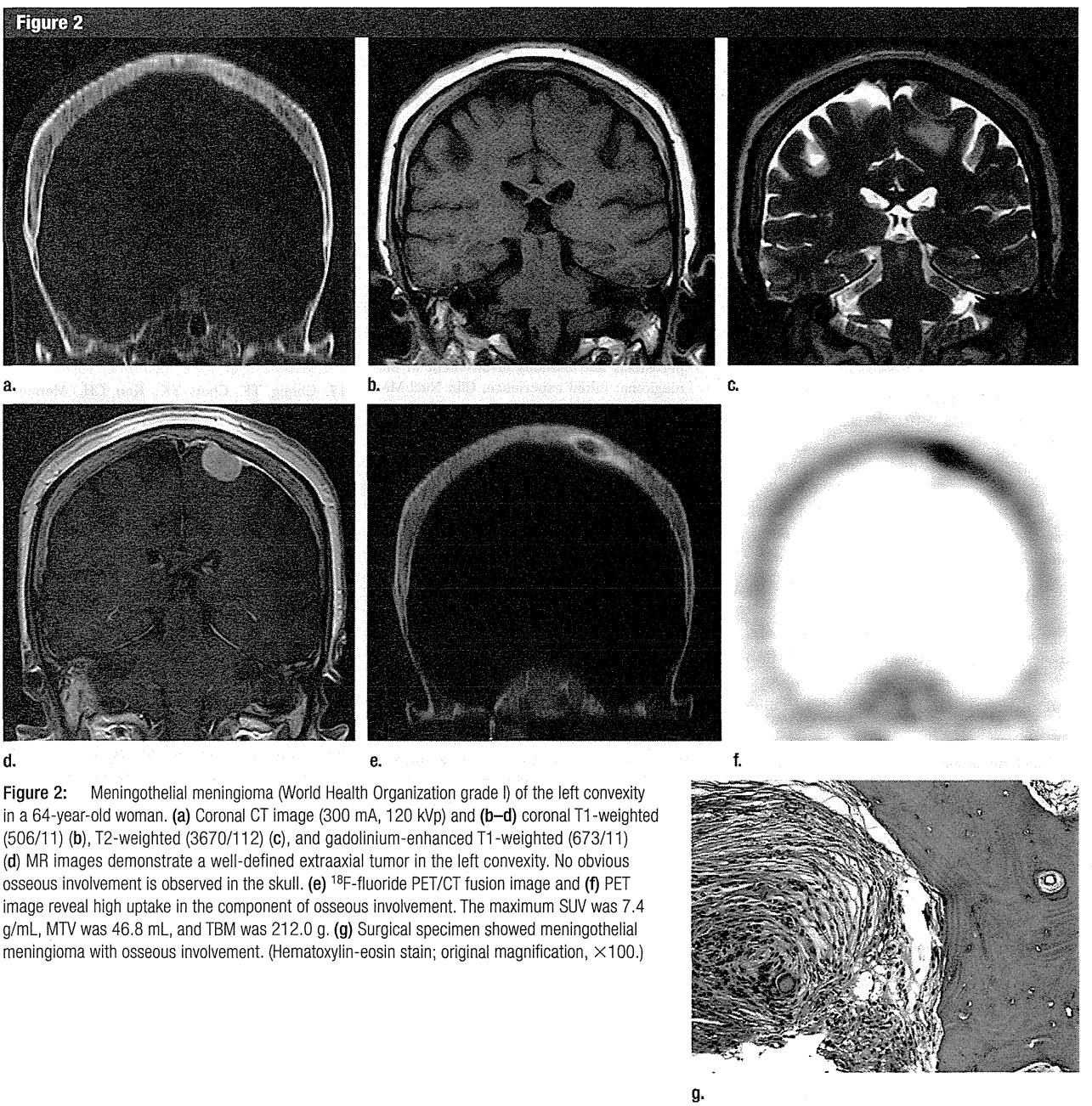

Figure 2: Meningothelial meningioma (World Health Organization grade I) of the left convexity in a 64-year-old woman. **(a)** Coronal CT image (300 mA, 120 kVp) and **(b–d)** coronal T1-weighted (506/11) (**b**), T2-weighted (3670/112) (**c**), and gadolinium-enhanced T1-weighted (673/11) (**d**) MR images demonstrate a well-defined extraaxial tumor in the left convexity. No obvious osseous involvement is observed in the skull. **(e)** ^{18}F-fluoride PET/CT fusion image and **(f)** PET image reveal high uptake in the component of osseous involvement. The maximum SUV was 7.4 g/mL, MTV was 46.8 mL, and TBM was 212.0 g. **(g)** Surgical specimen showed meningothelial meningioma with osseous involvement. (Hematoxylin-eosin stain; original magnification, ×100.)

In the clinical setting, drilling or sampling of bone, which may induce damage of neural tissue, is not always performed in tumors arising from the skull base or the tentorium cerebelli. Further prospective and comparative analysis of a large population with close follow-up with MR imaging after surgery is warranted. Furthermore, the precise mechanism of ^{18}F-fluoride uptake within the osseous lesions is not fully investigated. Thus, histopathologically based assessment comparing expression of osteopontin and BMP-4 with surgical specimen findings will be required (9,10).

In summary, we recommend preoperative imaging by using ^{18}F-fluoride PET/CT to detect occult osseous involvement in patients with meningioma. The precise mechanisms remain unclear, but our favored hypothesis is that patients may proceed directly to conventional surgery when ^{18}F-fluoride

Figure 3

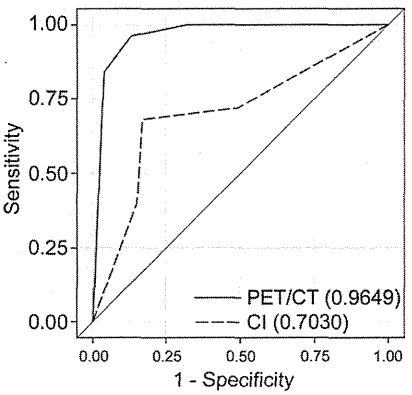

Figure 3: ROC curves of ^{18}F-fluoride PET/CT and conventional imaging *(CI)* for osseous involvement are presented. The mean A_z value of ^{18}F-fluoride PET/CT was significantly greater than that of conventional imaging (0.965 [rounded from 0.9649] ± 0.02 [standard error], with 95% confidence interval: 0.930, 1.000, vs 0.703 ± 0.066 [standard error], with 95% confidence interval: 0.574, 0.832), with $P < .0001$. Diagonal line = reference line ($A_z = 0.50$).

uptake within the skull is not abnormal. However, a positive finding at ^{18}F-fluoride PET/CT should prompt confirmation of osseous involvement by drilling or sampling of bone.

Acknowledgments: We thank Takashi Terauchi, MD, PhD, Division of Screening Technology and Development, Research Center for Cancer Prevention and Screening, National Cancer Center, Tokyo, Japan, and Jun Suenaga, MD, PhD, and Makoto Ohtake, MD, PhD, Department of Neurosurgery, Yokohama City University Graduate School of Medicine, Yokohama, Japan, for their help in collecting data.

Disclosures of Conflicts of Interest: U.T. disclosed no relevant relationships. **K.T.** disclosed no relevant relationships. **A.H.** disclosed no relevant relationships. **I.T.** disclosed no relevant relationships. **T.I.** disclosed no relevant relationships. **N.K.** disclosed no relevant relationships.

References

1. Terstegge K, Schörner W, Henkes H, Heye N, Hosten N, Lanksch WR. Hyperostosis in meningiomas: MR findings in patients with recurrent meningioma of the sphenoid wings. AJNR Am J Neuroradiol 1994;15(3):555–560.
2. Arana E, Diaz C, Latorre FF, et al. Primary intraosseous meningiomas. Acta Radiol 1996;37(6):937–942.
3. Hamilton BE, Salzman KL, Patel N, et al. Imaging and clinical characteristics of temporal bone meningioma. AJNR Am J Neuroradiol 2006;27(10):2204–2209.
4. Bikmaz K, Mrak R, Al-Mefty O. Management of bone-invasive, hyperostotic sphenoid wing meningiomas. J Neurosurg 2007;107(5):905–912.
5. Tateishi U, Tateishi K, Shizukuishi K, et al. 18F-Fluoride PET/CT allows detection of hyperostosis and osseous involvement in meningioma: initial experience. Clin Nucl Med 2013;38(3):e125–e131.
6. Lee JW, Kang KW, Park SH, et al. 18F-FDG PET in the assessment of tumor grade and prediction of tumor recurrence in intracranial meningioma. Eur J Nucl Med Mol Imaging 2009;36(10):1574–1582.
7. Akobeng AK. Understanding diagnostic tests. III. Receiver operating characteristic curves. Acta Paediatr 2007;96(5):644–647.
8. DeLong ER, DeLong DM, Clarke-Pearson DL. Comparing the areas under two or more correlated receiver operating characteristic curves: a nonparametric approach. Biometrics 1988;44(3):837–845.
9. Hirota S, Nakajima Y, Yoshimine T, et al. Expression of bone-related protein messenger RNA in human meningiomas: possible involvement of osteopontin in development of psammoma bodies. J Neuropathol Exp Neurol 1995;54(5):698–703.
10. Johnson MD, O'Connell MJ, Vito F, Pilcher W. Bone morphogenetic protein 4 and its receptors are expressed in the leptomeninges and meningiomas and signal via the Smad pathway. J Neuropathol Exp Neurol 2009;68(11):1177–1183.
11. Pieper DR, Al-Mefty O, Hanada Y, Buechner D. Hyperostosis associated with meningioma of the cranial base: secondary changes or tumor invasion. Neurosurgery 1999;44(4):742–746; discussion 746–747.
12. Jääskeläinen J. Seemingly complete removal of histologically benign intracranial meningioma: late recurrence rate and factors predicting recurrence in 657 patients—a multivariate analysis. Surg Neurol 1986;26(5):461–469.
13. Min JH, Kang SH, Lee JB, Chung YG, Lee HK. Hyperostotic meningioma with minimal tumor invasion into the skull. Neurol Med Chir (Tokyo) 2005;45(9):480–483.
14. Obeid F, Al-Mefty O. Recurrence of olfactory groove meningiomas. Neurosurgery 2003;53(3):534–542; discussion 542–543.
15. Ildan F, Erman T, Göçer AI, et al. Predicting the probability of meningioma recurrence in the preoperative and early postoperative period: a multivariate analysis in the midterm follow-up. Skull Base 2007;17(3):157–171.
16. Kanmaz B, Weissman DE, Akansel G, Kitapci M, Collier BD. Intraosseous meningioma: appearance on bone scintigraphy over five years. J Nucl Med 1993;34(6):961–962.
17. Cheng TF, Chen YK, Kao CH. Meningioma detected incidentally on early Tc-99m MDP whole-body imaging during a workup for breast cancer. Clin Nucl Med 2005;30(1):37–38.
18. Lim ST, Sohn MH. Intracranial meningioma with abnormal accumulation of Tc-99m MDP on bone scintigraphy: different intensities between reactive hyperostosis and tumor calcification. Clin Nucl Med 2001;26(5):475–477.
19. Lippitz B, Cremerius U, Mayfrank L, et al. PET-study of intracranial meningiomas: correlation with histopathology, cellularity and proliferation rate. Acta Neurochir Suppl (Wien) 1996;65:108–111.
20. Ghodsian M, Obrzut SL, Hyde CC, Watts WJ, Schiepers C. Evaluation of metastatic meningioma with 2-deoxy-2-[18F] fluoro-D-glucose PET/CT. Clin Nucl Med 2005;30(11):717–720.
21. Murakami M, Imahori Y, Kimura S, et al. Positron emission tomography elucidates transport system and tumor proliferation in meningiomas. Oncol Rep 2005;14(4):853–859.
22. Di Chiro G, Hatazawa J, Katz DA, Rizzoli HV, De Michele DJ. Glucose utilization by intracranial meningiomas as an index of tumor aggressivity and probability of recurrence: a PET study. Radiology 1987;164(2):521–526.
23. Iuchi T, Iwadate Y, Namba H, et al. Glucose and methionine uptake and proliferative activity in meningiomas. Neurol Res 1999;21(7):640–644.

Austin Journal of Neurosurgery

Austin Publishing Group

Open Access Full Text Article

Case Report

Oculomotor Nerve Schwannoma Presenting as an Entirely Cystic Homogeneous Mass on Magnetic Resonance Imaging: Case Report

Suenaga J*, Tateishi K, Takase H, Kanno H and Kawahara N

Department of Neurosurgery, Yokohama City University Graduate School of Medicine, Japan

***Corresponding author:** Suenaga J, Department of Neurosurgery, Yokohama City University Graduate School of Medicine, 3-9 Fukuura, Kanazawa-ku, Yokohama, Kanagawa 236-0004, Japan, Tel: +81-45-787-2663; Fax: +81-45-783-6121; Email: junjun@kvd.biglobe.ne.jp

Received: April 29, 2014; **Accepted:** June 05, 2014; **Published:** June 09, 2014

Abstract

A 79-year-old woman presented with left oculomotor nerve paresis. Initial Computed Tomography (CT) demonstrated an isodense cystic lesion 15 mm in diameter in the left crural and carotid cisterns. On Magnetic Resonance Imaging (MRI), the cyst was homogeneously hyperintense on both T_1- and T_2-weighted imaging with slight hemorrhage. Removal of the lesion was indicated, since the cyst was gradually enlarging and symptoms were progressing. Since the cyst was tightly attached to the oculomotor nerve, partial resection was performed. Pathology of the cyst wall revealed schwannoma with microhemorrhage. However, the residual tumor showed sudden bleeding 1 month later, so second surgery was performed to remove the tumor subtotally, leaving a small piece of residual capsule tightly adhering to the brainstem and internal carotid artery. Although oculomotor nerve schwannoma is rare, particularly presenting as a completely cystic mass, this diagnosis should be considered with such lesions. In addition, total or subtotal resection to prevent further enlargement or hemorrhage might be indicated, even in older patients.

Keywords : Oculomotor nerve schwannoma; Cyst formation; Intratumoral hemorrhage

Abbreviations

CT: Computed Tomography; MRI: Magnetic Resonance Imaging; DWI: Diffusion-Weighted Imaging; VS: Vestibular Schwannoma; CSF: Cerebrospinal Fluid; EMA: Epithelial Membrane Antigen; GKR: Gamma Knife Radiosurgery; FLAIR: Fluid-Attenuated Inversion-Recovery

Introduction

Oculomotor nerve schwannoma in the absence of neurofibromatosis is extremely rare, with only 56 cases previously reported in the literature [1-8]. According to a systematic review by Furtado et al. [2], the most common site of origin is in the cisternal segment of the oculomotor nerve. Although radiological diagnosis is usually made by Magnetic Resonance Imaging (MRI), precise diagnosis is often difficult, and differentiation from other tumors, including meningioma, dermoid cyst, craniopharyngioma, neurenteric cyst, and pituitary adenoma, is warranted. We recently treated a patient with an entirely cystic schwannoma originating from the oculomotor nerve in the crural cistern, which showed rapid growth and intratumoral hemorrhage. Such cystic tumors are extremely rare, and only two cases have been reported [5,6]. We report this case and review the pertinent literature, with particular focus on the radiological features.

Case Presentation

A 79-year-old woman presented to our clinic with left oculomotor nerve paresis. No special past or family history such as neurofibromatosis was noted. Computed Tomography (CT) showed an isodense cystic lesion 15 mm in diameter in the left crural cistern (Figure 1A). Tiny high-density niveau in this mass suggested hemorrhage in the cyst. No calcification or vessel anomaly was seen on CT angiography. MRI also revealed a homogeneous cystic mass, hyperintense on both T_1- and T_2-weighted imaging (Figure 1B, C). The tumor capsule did not show clear contrast enhancement. The mass was isointense to brainstem on Diffusion-Weighted Imaging (DWI). Due to the advanced age of the patient, we continued close observation; however, the cyst gradually enlarged and reached 22 mm in diameter after 6 months (Figure 2). The mass effect of the tumor on the left cerebral peduncle was increased, and oculomotor function gradually deteriorated. We finally decided to resect the tumor in order to decompress the brainstem, based on a tentative preoperative diagnosis of neurenteric cyst.

Through a left transsylvian approach, a cystic mass with grayish capsule was observed lateral to the internal carotid artery in the carotid cistern. The cyst was attached to the oculomotor nerve, suggesting a neural origin (Figure 3A). To preserve oculomotor function, partial resection of the cyst wall was performed, showing serous xanthochromic fluid as the cyst contents. In the pathological specimen, short spindle cells and a palisade-like pattern were observed on hematoxylin and eosin staining (Figure 3B). This and strong immunostaining for S-100 protein indicated schwannoma. Hemosiderin deposition was also confirmed by Berlin-blue stain, suggesting microhemorrhage in the tumor (Figure 3C).

After confirming successful evacuation of cyst fluid (Figure 4A-C), the patient was discharged without improvement of oculomotor nerve palsy. Five weeks later, however, the patient was readmitted

Citation: Suenaga J, Tateishi K, Takase H, Kanno H and Kawahara N. Oculomotor Nerve Schwannoma Presenting as an Entirely Cystic Homogeneous Mass on Magnetic Resonance Imaging: Case Report. Austin J Neurosurg. 2014;1(3): 1013.

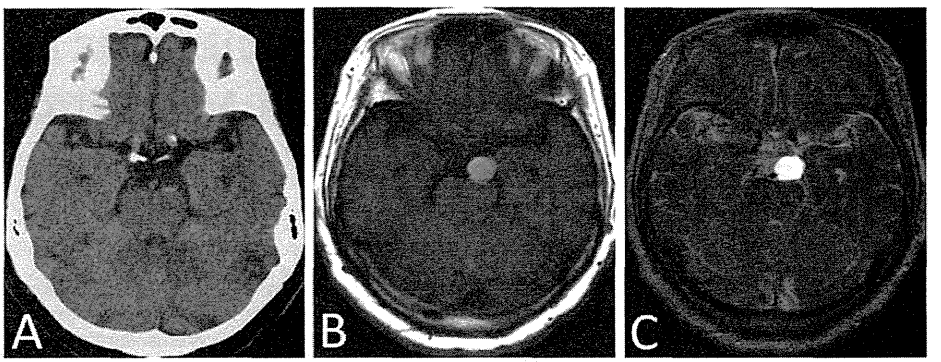

Figure 1: A) Axial unenhanced CT at presentation, showing a cystic lesion in the left crural cistern that is isodense to the cisternal space. **B, C)** Axial unenhanced MRI showing cystic and homogeneous mass. T_1-weighted imaging (B) shows a hyperintense mass. T_2-weighted imaging (C) shows extreme hyperintensity compared to brainstem. Tiny high-intensity niveau in this mass suggest hemorrhage in the cyst.

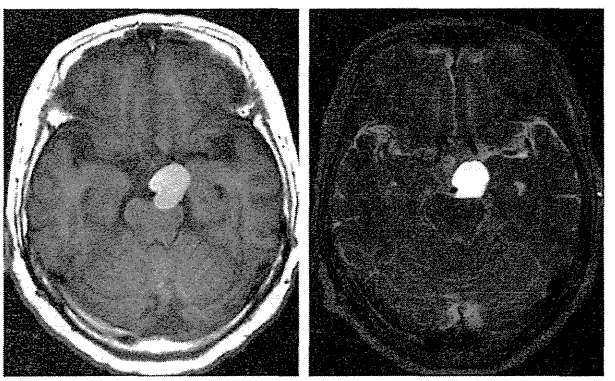

Figure 2: Seven months after initial onset, axial unenhanced MRI shows enlargement of the cyst. T_1-weighted imaging (left) and T_2-weighted imaging (right) also show homogeneous signal intensity and tumor size reaching 22 mm in diameter during this period.

with sudden onset of right hemiparesis, disturbance of consciousness, and complete left oculomotor palsy. Emergent CT demonstrated intratumoral hemorrhage from the residual tumor with midbrain compression and associated hydrocephalus (Figure 4D). Following ventriculo-peritoneal shunt for hydrocephalus, a second operation was performed for subtotal removal of the tumor with sacrifice of the oculomotor nerve, since the nerve was behind the enlarged tumor and hematoma, and was damaged severely with total loss of function preoperatively. A small piece of residual capsule tightly adhering to the brainstem and internal carotid artery was left intact after the procedure. After improvement of clinical condition, the patient was transferred to a rehabilitation hospital, 12 months after initial onset. And even up to 58 months after the procedure, the patient experienced no further rebleeding although there was a loss of complete oculomotor function.

Discussion

Schwannoma originating from the oculomotor nerve without neurofibromatosis is extremely rare. Such lesions are generally classified according to location, such as cisternal type (42%), cavernous sinus type (31%), cisterno-cavernous type (21%) and orbito-cavernous type (6%) [2,4]. The present case would be classified as cisternal type. The reported cases have mainly involved solid schwannoma, with the exception of two cases. One was mainly located in the lateral wall of the cavernous sinus and the tumor included a 10-mm round cyst [6]. The other was a relatively small mass, 15 mm in diameter and located in the cisternal portion, and exhibiting homogeneous hyperintensity on both T_1- and T_2-weighted imaging, as in the present case [5]. This latter case was preoperatively diagnosed as lipid-containing cystic craniopharyngioma, and subsequently identified pathologically as cystic schwannoma with microhemorrhage. These entirely cystic schwannomas, including the present case, may pose a diagnostic challenge.

A diagnostic clue in such cystic cases might be the presence of microhemorrhage, as observed in our case, since schwannoma is known to bleed intratumorally. In Vestibular Schwannoma (VS), progression of intratumoral microhemorrhage is reported to be associated with preoperative hearing loss [9]. In this study of 274 cases, most of the pathological specimen exhibited microhemorrhage, although major hemorrhage comprising >25% of the lesion was noted only in 23%. Several MRI studies have also suggested microhemorrhage in schwannoma [10-12]. More specific findings were reported by Thamburaj et al. who clearly demonstrated that 94% of VS showed signs of hemorrhage when examined on T2* imaging, suggesting this as a specific finding in differential diagnosis [13]. Such microhemorrhage, when repeated, has been considered to lead to cyst formation [14]. Indeed, cystic VS are reported to exhibit significantly more hemosiderin deposition than homogeneous solid VS [15]. In our case, repeated hemorrhaging, as verified by imaging and pathological findings (Figure 3C), was associated with cyst formation, which would also support this hypothesis.

Cyst itself, however, is not a specific finding in VS. According to the literature, the cyst formation comprises a mean of 5.7–48% of the VS, closer to 10% with more recent studies [16]. When associated with a large cyst, wall thickness and enhancement could offer diagnostic clues in favor of schwannoma when differentiating from other cystic lesions such as arachnoid cyst, neurenteric cyst, and epidermoid [16]. Based on these findings, our preoperative diagnosis was neurenteric cyst due to the homogeneous cyst and lack of wall enhancement.

Entirely cystic schwannomas with a lack of enhancement, particularly in the crural cistern, should be differentiated from other